

# CHEMISTRY

## A European Journal



### Accepted Article

**Title:** Au@TiO<sub>2</sub> Core-Shell Composites for the Photocatalytic Reduction of CO<sub>2</sub>

**Authors:** Anna Pougin, Georgios Dodekatos, Martin Dilla, Harun Tüysüz, and Jennifer Strunk

This manuscript has been accepted after peer review and appears as an Accepted Article online prior to editing, proofing, and formal publication of the final Version of Record (VoR). This work is currently citable by using the Digital Object Identifier (DOI) given below. The VoR will be published online in Early View as soon as possible and may be different to this Accepted Article as a result of editing. Readers should obtain the VoR from the journal website shown below when it is published to ensure accuracy of information. The authors are responsible for the content of this Accepted Article.

**To be cited as:** *Chem. Eur. J.* 10.1002/chem.201801796

**Link to VoR:** <http://dx.doi.org/10.1002/chem.201801796>

Supported by  
**ACES**

WILEY-VCH

# Au@TiO<sub>2</sub> Core-Shell Composites for the Photocatalytic Reduction of CO<sub>2</sub>

Anna Pougin<sup>[a],†</sup>, Georgios Dodekatos<sup>[b]</sup>, Martin Dilla<sup>[c]</sup>, Harun Tüysüz<sup>[b]\*</sup>, Jennifer Strunk<sup>[d]\*</sup>

**Abstract:** Au/TiO<sub>2</sub> catalysts in different geometrical arrangements were designed to explore the role of morphology and structural properties for the photocatalytic reduction of CO<sub>2</sub> with H<sub>2</sub>O in the gas-phase. The most active sample was a Au@TiO<sub>2</sub> core-shell catalyst with additional Au nanoparticles (NPs) deposited on the outer surface of the TiO<sub>2</sub> shell. CH<sub>4</sub> and CO are the primary carbon-containing products. Large amounts of H<sub>2</sub> are additionally formed by photocatalytic H<sub>2</sub>O splitting. Shell thickness plays a critical role. The highest yields were observed with the thickest layer of TiO<sub>2</sub>, stressing the importance of the semiconductor for the reaction. Commercial TiO<sub>2</sub> with and without Au NPs was less active in the production of CH<sub>4</sub> and CO. The enhanced activation of CO<sub>2</sub> on the core-shell system is concluded to result from electronic interaction between the gold core, the titania shell, and the Au NPs on the outer surface. The improved exposure of Au-TiO<sub>2</sub> interface contributes to the beneficial effect.

## Introduction

The photocatalytic reduction of CO<sub>2</sub> holds the potential to solve future shortages of mobile energy sources, whilst reducing the concentration of atmospheric CO<sub>2</sub>. Since the first reports on this reaction forty years have passed,<sup>[1]</sup> but a practical process and fundamental understanding is still in development.<sup>[2]</sup> In 2013, the yields of the main product, methane, obtained with most TiO<sub>2</sub>-based catalysts ranged between 0.1 and 5 μmol g<sub>Cat</sub><sup>-1</sup> h<sup>-1</sup>, which is far away from an industrial application.<sup>[2]</sup> One of the promising approaches to improve the activity of photocatalysts, and to possibly also gain understanding of the essential mechanistic steps, is the addition of noble metals, such as Au, to TiO<sub>2</sub>. From the field of classical heterogeneous catalysis, since the pioneering work of Haruta et al.<sup>[3]</sup> TiO<sub>2</sub>-supported Au nanoparticles are instead known for their properties in catalytic

oxidation reactions. In classical heterogeneous catalysis, parameters such as the interface between Au and TiO<sub>2</sub>,<sup>[4]</sup> the size and shape of Au,<sup>[3b,5]</sup> and the oxidation state of TiO<sub>2</sub><sup>[6]</sup> play a crucial role in the catalytic performance of the prepared catalyst.

In photocatalysis, modification of TiO<sub>2</sub> by deposition of noble metal nanoparticles on the surface is generally applied in order to enhance charge carrier separation over the Schottky barrier, and to better catalyze the reaction on the surface by lowering the activation energy.<sup>[7]</sup> This results in improved photocatalytic performances under UV light exposure. In a recent model study, some authors of the present work could confirm through infrared spectroscopy the generally accepted concept of photocatalytic activity enhancement by improved charge separation: For the photocatalytic 2-propanol oxidation in the gas phase, the role of gold in Au/TiO<sub>2</sub> was attributed to the removal of excess electrons otherwise accumulating in TiO<sub>2</sub>, and their further transfer onto the co-reactant oxygen.<sup>[8]</sup> In a photocatalyst system in which Au nanoparticles (NPs) had been photodeposited on TiO<sub>x</sub>/SBA-15, i.e. on a mesoporous silica (SBA-15) grafted with titanate (TiO<sub>x</sub>) species, the facilitation of an electron transfer reaction from the titania shell around the gold nanoparticles to gold and from there to the reactants was demonstrated to be a likely process.<sup>[9]</sup> Moreover, Au nanoparticle deposition proved to be a promising method in order to enable visible light absorption of TiO<sub>2</sub> due to the distinguishing properties of this noble metal. For instance, Dodekatos et al.<sup>[10]</sup> and Schünemann et al.<sup>[11]</sup> showed that selective oxidation of glycerol in the aqueous phase over TiO<sub>2</sub>- or SiO<sub>2</sub>-supported Au or AuCu nanoparticles can be improved by the aid of visible light irradiation during the thermally catalyzed reaction. The visible light was absorbed by the Au nanoparticles to enhance the catalytic performance. The origin of the light absorbing properties of the Au nanoparticles can be rationalized by the localized surface plasmon resonance (LSPR) effect.<sup>[12]</sup> In a simple mechanistic scheme, the LSPR can be explained by the collective oscillation of the conduction electrons on the surface of the metal nanoparticle induced by the interaction of the electrons with the electromagnetic field of the impinging light and the restoring Coulomb force of the positive nuclei of the metal.<sup>[13]</sup>

Apart from attributing enhanced photocatalytic performance to improved charge carrier separation and visible light absorption, different energy transfer mechanisms have been proposed for metal/semiconductor composites.<sup>[13b, 14]</sup> LSPR induces strong electromagnetic fields around the nanoparticle with higher intensities than the incident electric field for the initialization of the LSPR. The intensity of the field depends on the geometry and size of the metal nanoparticle and the extinction coefficient of its surroundings.<sup>[12-15]</sup> A resonantly enhanced near field in the surrounding medium arises in direct vicinity to the metal nanoparticle surface, which can be understood in terms of a concentrated light flux.<sup>[13a, 14]</sup> This may play a key role in photocatalysis,<sup>[13a]</sup> potentially also by local heating effects.<sup>[13c]</sup> In

- [a] Dr. A. Pougin  
Laboratory of Industrial Chemistry  
Ruhr-University Bochum  
44780 Bochum, Germany
- [b] Dr. G. Dodekatos, Dr. H. Tüysüz  
Max-Planck-Institut für Kohlenforschung  
45470 Mülheim/Ruhr, Germany  
Email: tueysuez@kofo.mpg.de
- [c] M. Dilla  
Max-Planck-Institute for Chemical Energy Conversion  
45470 Mülheim/Ruhr, Germany
- [d] Prof. Dr. J. Strunk  
Leibniz-Institute for Catalysis (LIKAT) at the University of Rostock  
18059 Rostock, Germany  
Email: jennifer.strunk@catalysis.de
- † Present address: Evonik Industries, Paul-Baumann-Str. 1, 45772 Marl, Germany

Supporting information for this article is given via a link at the end of the document.

another mechanism, sometimes referred to as “hot electron transfer”, the charge carriers are assumed to be directly injected from the metal to the semiconductor, which is similar to the mechanism described for dye sensitized photocatalysts.<sup>[13,14,16]</sup> It is, however, also possible that the surface chemistry of the noble metals exert a major influence on the catalytic surface processes, so that the enhancement is brought about predominantly by catalytic effects, and not by alterations in light absorption or charge carrier mobility. In any case, it is the nature of the semiconductor TiO<sub>2</sub> that determines major properties concerning the lifetime of the charge carriers. The dependency of charge carrier diffusion dynamics and TiO<sub>2</sub> particle size in Au/TiO<sub>2</sub> has been studied by Luchao Du et al.<sup>[17]</sup> They discovered the trend that with bigger TiO<sub>2</sub> particles the chances of electron-hole-recombination are decreased due to the longer diffusion length of electrons, and the catalyst is more efficient in a size range between 8 and 50 nm.

Many efforts have been devoted to utilizing the plasmonic properties for photocatalytic CO<sub>2</sub> reduction.<sup>[13b,18]</sup> For instance, Hou et al.<sup>[19]</sup> reported an enhancement in activity in photocatalytic CO<sub>2</sub> reduction over Au/TiO<sub>2</sub> in comparison to the bare support and attributed it to a positive influence from the surface plasmon. Two different mechanisms were assumed to be in operation, depending on whether the plasmon was excited with green light or whether the composite was irradiated with UV light.<sup>[19]</sup> Recently, a study conducted by some of the authors of the present work, performed under reaction conditions of highest purity, supports a possible influence of plasmonic effects in noble metal-modified TiO<sub>2</sub>. However, such effects were clearly noticeable only for Ag/TiO<sub>2</sub>, in line with the better overlap of the absorption spectra of TiO<sub>2</sub> with the plasmon resonance absorption of silver compared to that of gold.<sup>[20]</sup> Another study shows that when neither the wavelength of the plasmon resonance nor the absorption edge of the metal oxide is hit exactly, but instead a value in between is chosen, the activity is maximized.<sup>[21]</sup>

Although many studies have been reported where nanostructured core-shell materials with (mostly) noble metal cores and semiconductor shells were used to perform photocatalytic hydrogen generation from water<sup>[22]</sup> or pollutant degradation,<sup>[23]</sup> such kinds of materials were scarcely investigated for photocatalytic CO<sub>2</sub> reduction.<sup>[24]</sup> It is expected that the special morphology can influence the photocatalytic activity of the material. For example, Seh et al. showed that by changing the morphology of Au/TiO<sub>2</sub> nanostructures the photocatalytic performance for hydrogen evolution can be altered.<sup>[22f]</sup> Janus Au/TiO<sub>2</sub> nanostructures exhibited an improved activity compared to analogous core-shell nanostructures. Nonetheless, the core-shell structured materials were superior to simple Au/TiO<sub>2</sub> nanocomposites, where Au NPs were deposited on TiO<sub>2</sub> without any specified morphology. The high activities were attributed to the plasmonic electric fields caused by the Au NPs, which were more pronounced for large Au NPs (Janus and core-shell morphology). Furthermore, a stronger localization of the electric fields was calculated for the Janus nanostructure, which was consistent with the improved activity. Hence, the morphology plays a crucial role for the presented photocatalytic

applications and encouraged us to investigate Au/TiO<sub>2</sub> photocatalysts with core-shell morphology for the CO<sub>2</sub> reduction. In this contribution, TiO<sub>2</sub>-encapsulated Au nanoparticles are tested in the photocatalytic CO<sub>2</sub> reduction in the gas-phase under conditions of highest possible purity. Our reaction conditions exclude additional product formation from impurities. The geometry of the Au@TiO<sub>2</sub>-Au nanospheres consists of three levels: the Au core (~20 nm), surrounded by a TiO<sub>2</sub> shell (Au@TiO<sub>2</sub>), and additional Au nanoparticles (~3 nm) on the outer TiO<sub>2</sub> shell (Au@TiO<sub>2</sub>-Au). The thickness of the TiO<sub>2</sub> shell is varied (20, 11, and 8 nm) to study potential influences of a shielding of the metal core, and to identify the role of a well-established semiconductor structure for the photocatalytic process. All catalysts are prepared in two versions, with and without the additional Au nanoparticles on the outer surface of the TiO<sub>2</sub> shell, to judge upon the influence of exposed and encapsulated Au nanoparticles. In order to put all findings into perspective, the best catalysts were tested in an advanced gas chromatography (GC) system to detect all potential reaction products. A commercial Au/TiO<sub>2</sub> catalyst and two home-made Au/TiO<sub>2</sub> catalysts without core-shell structure were tested as references.

## Results and Discussion

### Structural characterization of the Au/TiO<sub>2</sub> core-shell samples

Representative TEM images of the samples Au@TiO<sub>2</sub>-08 and Au@TiO<sub>2</sub>-08-Au are displayed in Figure 1. In the image of sample Au@TiO<sub>2</sub>-08 (Figure 1 a and b) the TiO<sub>2</sub> shell thickness was measured in certain areas, with an average thickness of ~ 8 nm. The gold cores vary slightly in shape. Pure spheres and slightly elongated structures are observed. The rough diameter of the gold cores is ~20 nm, and they are clearly encapsulated by the TiO<sub>2</sub> shell. From Figure 1a and b, it is not possible to distinguish whether or not any part of the gold surface is still accessible to the surrounding atmosphere, but the predominant core-shell structure is unambiguously visible. In the TEM image

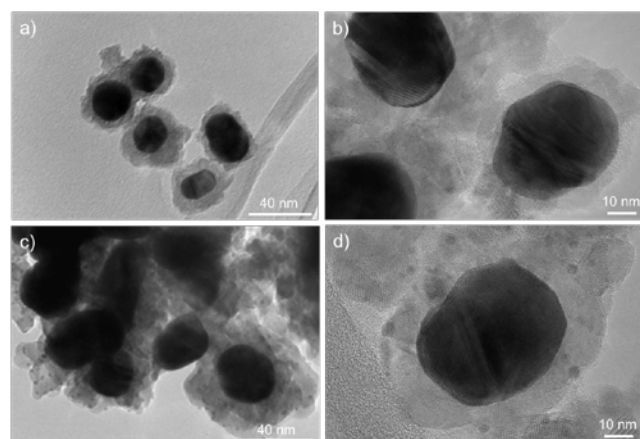


**Figure 1.** Representative TEM images of samples Au@TiO<sub>2</sub>-08 (a,b) and Au@TiO<sub>2</sub>-08-Au (c,d); the average shell thickness of about 8 nm and the

successful deposition of additional gold nanoparticles on the outside of the TiO<sub>2</sub> shell can be clearly identified.

of sample Au@TiO<sub>2</sub>-08-Au (Figure 1 c and d), the additional gold nanoparticles on the outer surface are detected. They are very uniform in size with an approximate diameter of 3 nm, being considerably smaller than the gold cores. In Figure 1c it can also be seen that some of the gold cores are not fully encapsulated but exhibit some Au surface possibly free of titania (e.g. particle in the center of the image). Representative TEM images of the other samples can be found in the supporting information (Figure S1 and S2). It appears that the gold nanoparticles on the outer shell cannot be distinguished anymore once the TiO<sub>2</sub> shell becomes too thick.

The XRD patterns of the Au@TiO<sub>2</sub> samples are shown in Figure 2. Three reflexes of the gold nanoparticles are observed, which are located at 38.1° (111), 44.3° (200) and 64.5° (220) 2 $\theta$ . The only crystalline TiO<sub>2</sub> phase detected in the samples is anatase; no indication for the presence of rutile or other metastable phases is evident. Of course, based on XRD data, the presence or absence of amorphous phases cannot be judged upon. Relative to the intensity of the most prominent reflection of gold, the reflections of titania become more pronounced the thicker the titania shell in the samples is. This is in accordance with the expectations. The increased reflections may be due to the increase in the amount of titania in the samples and/or due to an improved crystallinity of the titania shell. The analogous samples with additional Au nanoparticles on the TiO<sub>2</sub> surface show identical diffraction patterns (not shown).

In the UV-vis measurements shown in Figure 3, a certain "support effect" of the TiO<sub>2</sub> shell on the Au core becomes obvious. Upon increasing the shell thickness the plasmon resonance absorption of the Au core experiences a red shift.<sup>[25]</sup> While the maximum is observed at 604 nm for the sample Au@TiO<sub>2</sub>-08 with the thinnest TiO<sub>2</sub> shell, it is shifted to 630 and 648 nm for TiO<sub>2</sub> shells of 11 and 20 nm, respectively. The red shift in combination with noble metal particle enclosure has already been studied by Kelly et al.<sup>[25]</sup>

**Figure 2.** XRD patterns of the Au@TiO<sub>2</sub> samples with different shell thickness (without extra Au deposition on the TiO<sub>2</sub> shell).

More information on the surface and adsorption properties of the samples is gathered with diffuse reflectance infrared Fourier transform spectroscopy (DRIFTS). Figure 4 shows the full range spectra of the as made samples after a mild drying procedure in inert gas. Pretreatment was kept minimal, in order to learn as much as possible on the initial state of the samples. In the region between 3800 and 3600 cm<sup>-1</sup>, three different hydroxyl groups can be distinguished, located at 3736 cm<sup>-1</sup>, 3675 cm<sup>-1</sup> and 3630 cm<sup>-1</sup>, which are assigned to two different terminal Ti<sup>IV</sup>-OH groups on anatase (3736, 3675 cm<sup>-1</sup>),<sup>[26]</sup> and a bridging OH group between two titanium cations (3630 cm<sup>-1</sup>).<sup>[26, 27]</sup> When additional gold nanoparticles are deposited on the outer surface, the amount of terminal OH groups seems to be slightly higher relative to the bridging OH groups. This appears reasonable, considering that some nearest neighbor Ti cations may be covered by the deposited gold nanoparticles instead of by an OH group. Slight changes in the surface coverage with hydroxyl groups in response to gold deposition are also a piece of evidence that the outer gold nanoparticles are actually attached to the titania shell.

In the region of ~1700 to ~1300 cm<sup>-1</sup> (Figure 4, left) a variety of (bi)carbonate species is detected on all samples, together with adsorbed water (~1622 cm<sup>-1</sup>). The presence of (bi)carbonate species is expected, because the samples have been synthesized from organic precursors. Upon calcination, the precursors are oxidized to CO<sub>2</sub>, which may then readsorb and may even be incorporated into the structure. Furthermore, samples have not been dried or cleaned prior to the IR measurements, so it is likely that physisorption of moisture and CO<sub>2</sub> from ambient air had taken place when samples were introduced into the DRIFTS sample cell. The CH<sub>x</sub> impurities detected on some samples, indicated by bands in the region between 3000 and 2700 cm<sup>-1</sup>, presumably also originate from residual precursors. Additional to the expected surface impurities, linearly bound CO<sub>2</sub> is observed with a band at ~2346 cm<sup>-1</sup>.<sup>[28]</sup> The observation of this band is surprising, because such

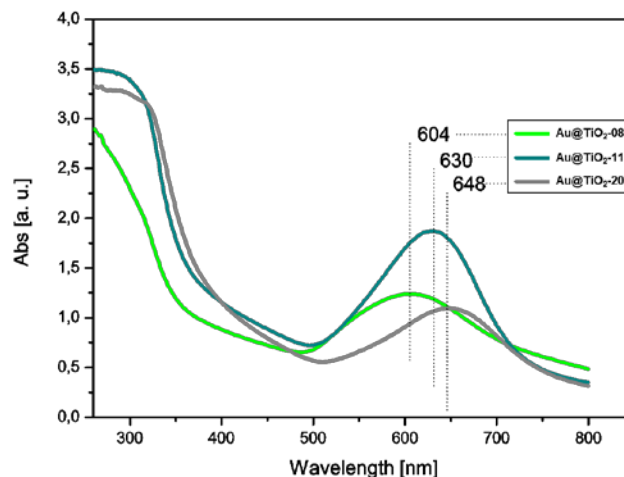
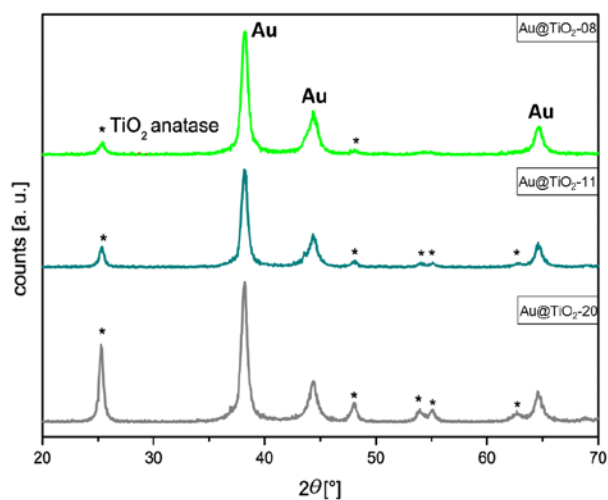


**Figure 3.** UV-vis spectra of Au@TiO<sub>2</sub> samples (without Au decoration on the outside of the TiO<sub>2</sub> shell).

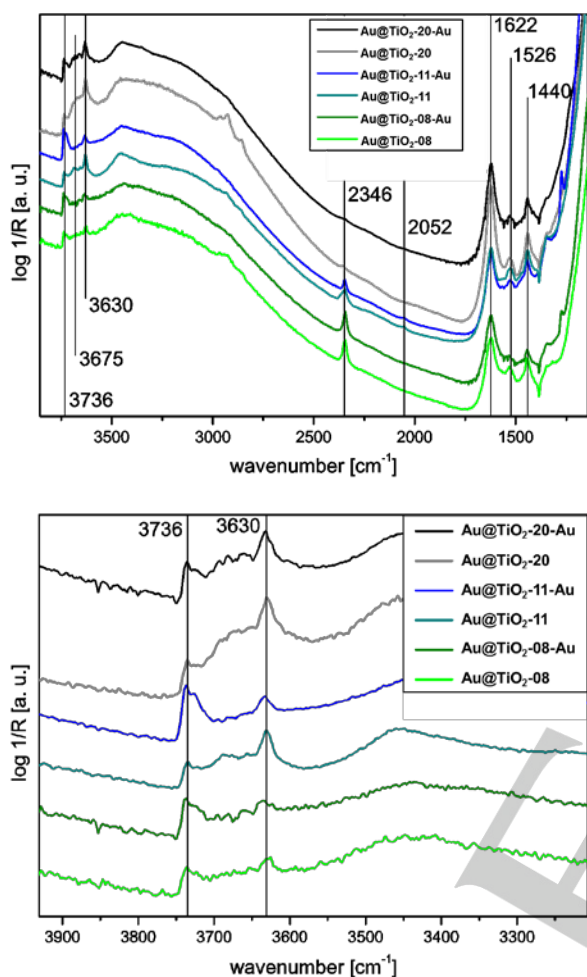


**Figure 4.** DRIFT spectra of as made Au@TiO<sub>2</sub> and Au@TiO<sub>2</sub>-Au samples after purging in inert gas; top: full range spectra; bottom: zoom into hydroxyl group region.

species are usually only observed during low-temperature adsorption. The same is true for the very weak band observed at 2052 cm<sup>-1</sup>, which is assigned to CO bound to slightly negatively charged Au. The band shift to such low wavenumbers may be explained by the Stark effect or by metal back-donation into antibonding orbitals of the adsorbed CO.<sup>[29]</sup> The adsorption of CO and/or CO<sub>2</sub> onto TiO<sub>2</sub> and Au/TiO<sub>2</sub> is usually known to be very unstable and it is thus usually performed at low temperatures of ~60 to 110 K,<sup>[30]</sup> and rarely at room temperature.<sup>[29]</sup> The observations are different in the present work. Figure S3 (Supporting Information) shows that both species cannot be removed from Au@TiO<sub>2</sub> samples even with a heat treatment up to 200 °C. In fact, the band intensity is not even decreased to the slightest extent. It is thus concluded that the adsorbed CO and CO<sub>2</sub> species are not present on the

surface of the materials, but are, instead, integrated (trapped) into their bulk structure. This is supported by the lack of any changes in these bands after the photocatalytic reaction (Figure S4), which also proves that these species are not consumed during the photocatalytic process. For a further discussion of the peculiar bands of “trapped” CO<sub>2</sub> and CO, please see the Supporting Information. It is interesting to note that at least some of the gold present in the samples must be slightly negatively charged, as evidenced by the position of the stretching vibration of adsorbed CO (2052 cm<sup>-1</sup>).

#### Activity tests in photocatalytic CO<sub>2</sub> reduction

Preliminary photocatalytic tests of all samples in photocatalytic CO<sub>2</sub> reduction are displayed in Figure 5. All samples have been measured under identical batch reaction conditions and have been thoroughly cleaned photocatalytically prior to the reaction with CO<sub>2</sub>. The gas composition in all cases consisted of 1.5% CO<sub>2</sub> and ~6000 ppm H<sub>2</sub>O in ultrapure Helium. In this measurement series, the used GC system generally allows to detect methane, methanol and higher hydrocarbons from concentrations as low as ~1 ppm. H<sub>2</sub> and CO cannot be detected with this device.

From all detectable components, methane was the main product formed on all samples (Figure 5). While traces of ethane were detected, methanol was never observed. It is very obvious that sample Au@TiO<sub>2</sub>-20-Au is much more active than all other samples used in this study. Considering the activity of all six samples, it seems to be a general trend that methane productivity increases with a thicker TiO<sub>2</sub> shell, and also with additional gold nanoparticle deposition on the outer TiO<sub>2</sub> surface. It is thus straightforward to expect sample Au@TiO<sub>2</sub>-20-Au to be the best one, because it features both a fairly thick TiO<sub>2</sub> shell and gold nanoparticles on the outer surface.

To put the results into perspective, in-depth studies were performed with the two most active samples with the thickest TiO<sub>2</sub> shell, Au@TiO<sub>2</sub>-20 and Au@TiO<sub>2</sub>-20-Au. Measurements were conducted in an identical set-up, but the gas analysis was performed with a different GC. This advanced GC analyzes the gas atmosphere with a barrier discharge ionization detector

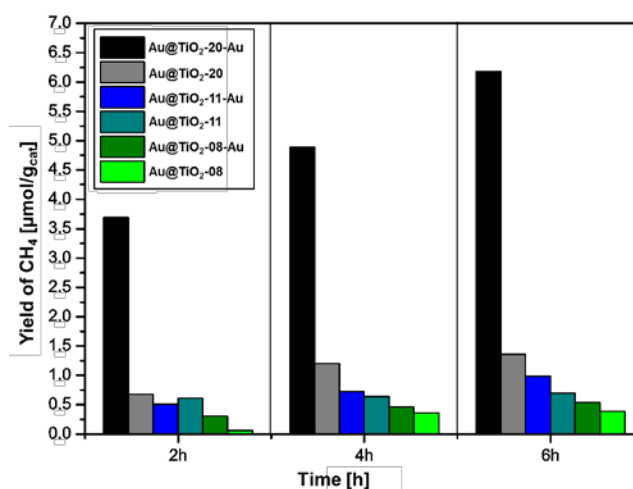


**Figure 5.** Activity screening for methane formation on all Au@TiO<sub>2</sub> and Au@TiO<sub>2</sub>-Au samples in photocatalytic CO<sub>2</sub> reduction (1.5%CO<sub>2</sub>, ~6000 ppm H<sub>2</sub>O) over 6 h.

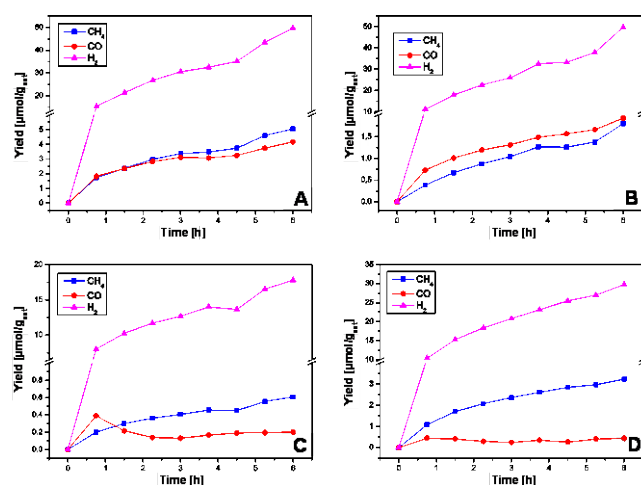


**Figure 6.** Results of activity testing in CO<sub>2</sub> reduction with 6,000 ppm of H<sub>2</sub>O and 1.5 % CO<sub>2</sub> over a course of 6 h, 200 W Hg/Xe lamp with IR filter; (A) Au@TiO<sub>2</sub>-20-Au, (B) Au@TiO<sub>2</sub>-20, (C) AUROLite™, (D) Au/P25.

(BID). With this GC it was possible to quantify not only the formed amounts of methane and ethane, but also of CO and H<sub>2</sub>. One GC sampling every 45 min is possible. The produced amounts were recorded both during the cleaning step and in the photocatalytic reaction. The results of the initial batch cleaning procedures are displayed and reported in the supporting information (Figure S5). After the batch cleaning procedures, the samples were continuously exposed to cleaning treatment in the flow mode. Monitoring of desorbing species is not possible under flow conditions, but after a few hours of flow cleaning, the reactor is closed off (batch cleaning) and desorbing contaminants are accumulated for 1 hour before a GC sampling is performed. This process is repeated until the desorbing amounts of CO, CH<sub>4</sub>, and H<sub>2</sub> were <0.06 μmol/g<sub>cat</sub>. Subsequently, the reactor was filled with the CO<sub>2</sub>-containing gas mixture (1.5% CO<sub>2</sub>, 6000 ppm H<sub>2</sub>O in He), and the product formation under batch CO<sub>2</sub> reduction conditions was recorded with the advanced GC for a period of six hours. Apart from the two core-shell systems, an industrial AUROLite™ catalyst and the two homemade Au/TiO<sub>2</sub> catalysts with conventional arrangement of gold nanoparticles were also tested (cleaning was performed identically for all samples; results of the AUROLite™ catalyst are shown in Figure S5 as an example). The results of the two Au@TiO<sub>2</sub> core-shell systems, the commercial AUROLite™ and the Au/P25 sample are displayed in Figure 6. The results of the activity test with the home-made Au/anatase sample and a reference measurement with pure P25 is displayed in the supporting information (Figure S6). Using the advanced GC for product analysis, it becomes obvious that the main product from photocatalytic reactions is not derived from CO<sub>2</sub>. Instead, H<sub>2</sub> is formed in major quantities with all samples.

Even though all tested catalysts have a different structural combination of Au in and/or on TiO<sub>2</sub> with differing nanoparticle geometries, the product profiles during CO<sub>2</sub> reduction are largely similar. H<sub>2</sub> is formed as overall main product, and CH<sub>4</sub> and CO are the main carbon-containing products.

There are two significant differences between the Au@TiO<sub>2</sub> core-shell samples and the commercial Au/TiO<sub>2</sub> samples. Firstly, the overall amount of products (related to catalyst mass) is larger for the core-shell samples, in particular with respect to H<sub>2</sub>. Secondly, the core-shell samples also produce significant amounts of CO, while this product is almost completely absent for the Au/TiO<sub>2</sub> catalysts with conventional geometry. We assign this to the high CO oxidation activity of the conventional or commercial Au/TiO<sub>2</sub> catalysts already at low temperatures. This is supported by the temporal evolution of CO: While some CO is formed initially, it disappears again over the course of time; likely because it is reoxidized to CO<sub>2</sub>.

Although a different GC is used for the detailed measurements, the relative trends in methane production of the two different Au@TiO<sub>2</sub> core-shell systems are fairly well reproduced. Sample Au@TiO<sub>2</sub>-20-Au, with additional gold nanoparticles on the outside of the shell, is roughly three times as active for the formation of methane as the sample Au@TiO<sub>2</sub>-20 without the additional external gold nanoparticles. With the other GC (Figure 4) this ratio was about 4. There are certain deviations in absolute numbers. In the first measurement with sample Au@TiO<sub>2</sub>-20-Au (Figure 4), the amount of methane formed over the course of six hours was roughly 6.0 μmol/g<sub>cat</sub>. In the measurement with the GC containing the BID, methane production within six hours amounted to 5.05 μmol/g<sub>cat</sub>. For sample Au@TiO<sub>2</sub>-20, methane production was ~1.5 and 1.8 μmol/g<sub>cat</sub> in the two measurements, respectively. Rather than being measurement errors, the deviations may be due to a differing sample orientation towards the incoming light. This has been confirmed recently for pure TiO<sub>2</sub>.<sup>[31]</sup> In summary, the relative activity of the samples can be considered to be well reproducible.

#### Discussion

The structural characterization of the samples by means of TEM and XRD confirms the core-shell structure of the materials and the presence of TiO<sub>2</sub> in the anatase phase. The thickness of the titania shell has an influence on the plasmon absorption of the central gold core, which shifts to higher wavelength (lower energy) with thicker TiO<sub>2</sub> shell. Although the additional gold nanoparticles on the outer surface are not detectable by either XRD or UV-Vis, they are clearly visible in the TEM images for the Au-TiO<sub>2</sub>-08-Au sample (Figure 1B). For all samples, the changes in the hydroxyl group coverage observed by DRIFTS are an indication for their anchoring to the outer TiO<sub>2</sub> shell. At least some of the gold in the samples must be partially negatively charged, as evidenced by the position of the weak vibrational band of adsorbed CO, clearly visible for samples Au@TiO<sub>2</sub>-11 and Au@TiO<sub>2</sub>-11-Au.

All samples are active in photocatalytic CO<sub>2</sub> reduction, with the yields of CH<sub>4</sub> increasing both with a thicker TiO<sub>2</sub> shell and with the addition of the small nanoparticles on the outer shell. In this

respect, the sample with the thickest shell and the additional outer nanoparticles (Au@TiO<sub>2</sub>-20-Au) is by far the most active sample for the formation of CH<sub>4</sub>. This was confirmed by two separate measurements using two different gas chromatographs for analysis. In-depth studies of the two most active samples (Au@TiO<sub>2</sub>-20 and Au@TiO<sub>2</sub>-20-Au), conducted using an advanced GC, reveal that CH<sub>4</sub> is not the overall main product. Instead, hydrogen is the predominant product on all samples studied here, with the yields of H<sub>2</sub> exceeding those of CH<sub>4</sub> by roughly an order of magnitude. Hydrogen is also the main product with the conventional Au/TiO<sub>2</sub> reference samples, but for all conventional Au/TiO<sub>2</sub> samples the yields of CH<sub>4</sub> are smaller than those observed for the most active Au@TiO<sub>2</sub>-Au sample. Concerning the product distribution, the most striking difference between the conventional Au/TiO<sub>2</sub> photocatalysts and the core-shell photocatalysts is that the latter also form CO, while this product is hardly observed on the conventional catalysts. This is attributed to the high activity of the conventional Au/TiO<sub>2</sub> catalysts in low-temperature CO oxidation, the actual target reaction for which this photocatalyst system has been developed. The new core-shell system is thus beneficial in two respects: Total yields of valuable products are larger, and CO is observed as an additional product.

UV-vis measurements show that light absorption is governed both by the Au nanoparticle in the core and the semiconducting titania shell (Figure 3). The additional small gold nanoparticles on the outer surface do not exert a significant influence on light absorption, because they did not cause a visible change in the UV-Vis spectra (not shown). Considering only the Au@TiO<sub>2</sub> samples without additional gold nanoparticles on the outer shell in a first step, the well-developed structure of the semiconductor TiO<sub>2</sub> in the shell is an important parameter for high activity of the core-shell systems under UV+vis illumination. One reason may be a better developed crystal structure (less defects) in the thicker shell. A possible enhancing influence of "hot electron transfer" from the gold core to the titania shell seems less relevant, since such a process is expected to occur most likely in the samples with the thinnest titania shell (8 nm).

A further decoration with Au nanoparticles on the outer TiO<sub>2</sub> surface results in a remarkable three- to fourfold increase in activity for methane formation in the case of the thickest TiO<sub>2</sub> shell. This is clear evidence that the nanoparticles on the outer surface are much more relevant for photocatalytic CO<sub>2</sub> reduction than the gold core. Both a plasmonic effect of the small external nanoparticles, as well as improved catalytic properties due to the exposed gold surface on the small nanoparticles may cause this significant increase in activity.

The results of the activity tests with the conventional Au/TiO<sub>2</sub> reference samples show that a pure catalytic effect alone cannot explain the higher activity. The conventional catalysts feature exposed gold nanoparticles of similar size, but total photocatalytic activity is lower and product distributions are altered, in particular with respect to the lack of CO production. The same observation also rules out plasmonic or structural effects related to the small size of the nanoparticles on the outer shell as sole reason for the observed differences. If those were the decisive factor, the reference samples should behave similar

to the core-shell samples. A simple effect of a larger amount of gold in the core-shell samples is also unlikely: The Au/P25 sample with a much higher gold loading compared to the Au/anatase samples showed the same trends as the other Au/TiO<sub>2</sub> reference samples, in which predominantly H<sub>2</sub> and almost no CO was formed. Instead, it seems that three aspects have to work together for the significantly improved photocatalytic activity for the formation of CH<sub>4</sub> and CO, namely (i) a structurally well-developed anatase TiO<sub>2</sub> shell, (ii) a gold core and (iii) exposed gold nanoparticles on the outer surface. In such a system, the combination of Au and TiO<sub>2</sub> shows fundamental differences in the (photo)catalytic properties, evidenced particularly by the inability of the core-shell system to (re)oxidize CO. Whereas in all conventional Au/TiO<sub>2</sub> catalysts the initially formed CO disappears again within the first few hours of the experiment, the amounts of CO formed with the core-shell samples roughly equal the produced amounts of CH<sub>4</sub>. The different behavior may originate from structural and electronic factors. Electromagnetic fields caused by light irradiation of the core-shell metal-semiconductor-metal structure may be very different from those caused in conventional Au/TiO<sub>2</sub> catalysts. Furthermore, the interface structure may be rather different in the core-shell system compared to samples prepared via the colloidal deposition route, in which reduction and rutilization of the interface has recently been observed.<sup>[32]</sup>

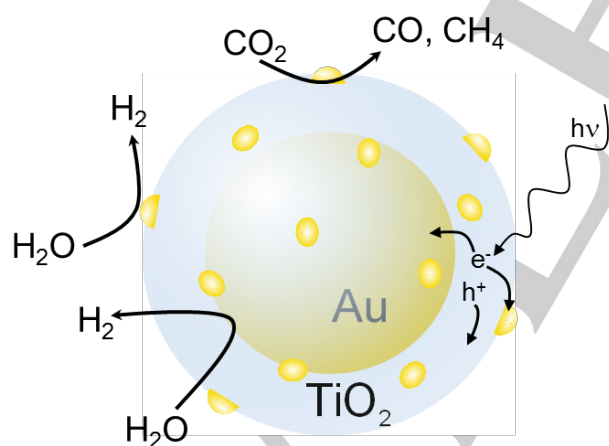
No mechanistic studies were conducted here, but the roughly equal amounts of CO and CH<sub>4</sub> formed photocatalytically may be indicative for the decomposition of a common intermediate in the mechanism. One option may be acetaldehyde, suggested previously as intermediate on bare TiO<sub>2</sub>.<sup>[33,37]</sup> It must be noted that the mechanism of CH<sub>4</sub> formation on TiO<sub>2</sub> is still under debate, particularly because some of the proposed elementary steps are thermodynamically not possible on bare TiO<sub>2</sub>, such as the formation of the CO<sub>2</sub> anion radical located at -1.9 eV on the electrochemical energy scale. In thermal catalysis with a Au/TiO<sub>2</sub> system it was found that acetaldehyde strongly interacts with the perimeter site of Au nanoparticles on TiO<sub>2</sub>.<sup>[34]</sup> If such an interaction also takes place during the photoreaction, acetaldehyde could be stabilized better with the Au@TiO<sub>2</sub>-20-Au catalyst compared to the Au@TiO<sub>2</sub>-20 catalyst, because the former has more Au nanoparticle-TiO<sub>2</sub> interface. According to Shkrob et al.,<sup>[33]</sup> under reaction conditions acetaldehyde breaks apart and forms CO and CH<sub>4</sub>. This would explain the product distribution observed for Au@TiO<sub>2</sub>-20-Au and Au@TiO<sub>2</sub>-20, where CO and CH<sub>4</sub> appear in a ratio close to 1 (Figure 6). The decomposition of an intermediate such as acetaldehyde might occur similarly on the conventional Au/TiO<sub>2</sub> catalysts, such as AUROLite™ and Au/P25 (Figure 6), but CO is quickly oxidized to CO<sub>2</sub> and does not show the same time profile as for the Au@TiO<sub>2</sub>-Au catalysts. Further insight into this issue may be obtained in future studies.

The results obtained here also indicate that H<sub>2</sub>, instead, can be formed photocatalytically under UV+Vis illumination on any accessible gold surface, regardless whether this surface belongs to the gold core or to the small nanoparticles on the outer surface. Since the amounts of H<sub>2</sub> formed on samples Au@TiO<sub>2</sub>-20-Au and Au@TiO<sub>2</sub>-20 are almost equal, the Au core seems to

have the dominant effect in both cases. In the reference samples, both a higher gold loading (as in Au/P25) and a larger size of the gold nanoparticles (as in Au/anatase) seem to influence the yields of  $H_2$  favorably, because in both cases more  $H_2$  is obtained compared to the commercial AUROLite™ catalyst. Within the first 45 min the largest increase in  $H_2$  formation can be detected, whereby after that period the formation is slowing down. Since the formation of all products observed in the present study occurs by processes consuming only electrons, this decreasing production rate of  $H_2$  for all tested samples (Figure 6) can be explained by the lack of an efficient hole consuming reaction, that is, the lack of formation of gaseous dioxygen. As has been described previously for bare  $TiO_2$ ,<sup>[31,37]</sup> instead of the formation of  $O_2$  in the gas phase, oxygen-derived species remain on or in the photocatalyst. The presence of those species eventually favors the back reaction, that is, oxidation of the formed hydrocarbons and hydrogen to  $CO_2$  and  $H_2O$ . Further studies on the fate of the holes are in progress and will be reported at a later time.

Our observations are summed up in Figure 7, which provides a schematic representation of the mode of action of the whole core-shell system. Charge carriers are generated by photoexcitation of the semiconductor, that is, the  $TiO_2$  shell. While the hole presumably remains and reacts on or in the  $TiO_2$  shell (and is not further considered here), the electron migrates either to the gold core or to the Au NPs on the outer  $TiO_2$  shell. The reduction of  $CO_2$  to CO and  $CH_4$  likely occurs on the interface of the Au NPs exposed on the outer  $TiO_2$  shell. The formation of hydrogen, on the other hand, can proceed on any exposed gold surface, both on the outer nanoparticles and the gold core.

**Figure 7.** Schematic representation of the mode of action of the core-shell



Au@TiO<sub>2</sub>-Au system.

## Conclusions

In this work Au@TiO<sub>2</sub>-Au catalysts with core-shell morphology were found to be superior to conventional Au/TiO<sub>2</sub> catalysts in the photocatalytic reduction of CO<sub>2</sub>. CH<sub>4</sub> and CO were the main carbon-containing products, and significant amounts of H<sub>2</sub> are

additionally formed. The sample with the thickest TiO<sub>2</sub> shell was most active, indicating a major role of the well-developed semiconductor structure in the reaction. Plasmonic field effects or a “hot electron transfer” from the gold core seem to be of minor importance, but may affect the reactivity of the small gold nanoparticles on the outer TiO<sub>2</sub> shell. The improved formation of carbon-containing products is attributed to an electronic interaction and a synergetic effect of all three structural features: (i) the thick TiO<sub>2</sub> shell, (ii) the gold core, and (iii) the Au NPs on the outside. In this arrangement, the latter lose their ability to rapidly oxidize CO at low temperature, so this product is stable on the core-shell system. CO and CH<sub>4</sub> formation in a ~1:1 ratio may indicate that both products originate from a common intermediate. H<sub>2</sub> formation is instead observed to a similar extent on all samples, indicating that this reaction can proceed on any accessible gold surface, and no particular geometry is needed.

## Experimental Section

### Preparation of Au@TiO<sub>2</sub>

Au@TiO<sub>2</sub> core-shell systems were synthesized based on a method reported elsewhere<sup>[22]</sup>, which was modified by our group. Au nanoparticles used as the core material were prepared by the well-known Turkevich method via citrate reduction. HAuCl<sub>4</sub> · 3 H<sub>2</sub>O (108 mg, 0.274 mmol, Sigma-Aldrich, ≥ 99.9 %) was dissolved in H<sub>2</sub>O (180 mL, millipore Q), heated to 115 °C and kept boiling for 15 min. Subsequently, sodium citrate dihydrate (180 mg in 5 mL H<sub>2</sub>O, Sigma-Aldrich) was quickly added into the vortex of the stirred solution. The mixture is boiled under reflux for 30 min and, subsequently, cooled down. Aqueous hydroxypropyl cellulose (300 mg dissolved in 15 mL H<sub>2</sub>O, Sigma-Aldrich) is added and the solution is stirred overnight. Gold nanoparticles with mean particle diameters of 20 nm can be obtained by this procedure. The aqueous gold solution is concentrated via centrifugation (final volume 25 mL) and mixed with isopropanol (90 mL, Sigma-Aldrich, 99.9 %) in a 250 mL round bottom flask. Aqueous NH<sub>3</sub> (3 mL, Sigma-Aldrich, 28 – 30 wt.%) is added to the dispersion and stirred vigorously for 15 min. Titanium diisopropoxide bis(acetylacetonate) (144 μL in 10 mL isopropanol for 8 nm shell, Aldrich, 75 wt.% dissolved in isopropanol) is slowly added into the vortex by a syringe pump and the mixture is further stirred overnight at RT. The material is washed twice with deionized water. Subsequently, the purple powder is dried at 90 °C for 1.5 h and calcined for 1 h at 500 °C (heating ramp: 4 °C min<sup>-1</sup>). Samples are denoted as Au@TiO<sub>2</sub>-X, where X indicates the thickness of the TiO<sub>2</sub> shell in nanometers. For the variation of the shell thickness, only the amount of the titania precursor was varied, while all other synthesis parameters were kept constant.

### Preparation of Au@TiO<sub>2</sub> decorated with Au nanoparticles

The decoration with Au nanoparticles on top of the Au@TiO<sub>2</sub> core-shell materials was achieved by a facile deposition-precipitation method with urea reported by Zanella et al.<sup>[35]</sup> Au@TiO<sub>2</sub> (20 mg) is dispersed in water (10 mL, millipore Q) together with urea (0.252 g, Fluka) and the desired amount of HAuCl<sub>4</sub> · 3 H<sub>2</sub>O for a total metal loading of 1 wt% at the outer TiO<sub>2</sub> surface. The mixture is then heated up to 90 °C and stirred for 4 h. The material is washed three times with deionized water and dried for 2 h at 50 °C under vacuum. The dried samples are then further calcined at 300 °C for 4 h (heating ramp: 2 °C min<sup>-1</sup>). Resulting samples are denoted as Au@TiO<sub>2</sub>-X-Au where X indicates the thickness of the TiO<sub>2</sub> shell in nanometers. An overview can be found in Table S1.

### Preparation of Au/TiO<sub>2</sub> reference samples

Gold nanoparticles with an average diameter of 4 nm were deposited on different commercial TiO<sub>2</sub> samples using the colloidal deposition method. The synthesis using the commercial anatase material (~300 m<sup>2</sup>/g, *Huntsman P&A Germany*) is reported in detail in a recent contribution.<sup>[32]</sup> The synthesis of the Au/P25 catalyst was performed similarly, using commercial TiO<sub>2</sub> P25 (~50 m<sup>2</sup>/g, *Evonik Industries*). The gold loading on the anatase support was adjusted to 1 wt%. On the P25 support, the loading of gold was 7.5 wt%. A commercial catalyst (AUROLite™, 1.5 wt% Au on TiO<sub>2</sub>, *STREM Chemicals*) was tested as reference. An overview over all samples studied in this contribution can be found in the supporting information (Table S1 and S2).

### Activity Testing in Photocatalytic CO<sub>2</sub> Reduction

The activity tests were performed in a home-made, metal-sealed, vacuum-tight photoreactor. A detailed description can be found elsewhere.<sup>[36]</sup> The full spectrum of a 200 W Hg/Xe lamp is used to irradiate the photocatalyst (UV+Vis), but the IR part is removed by an IR water filter attached in front of the lamp output lens to prevent heating of the sample through the beam. The IR filter is cooled by a cryostat providing a circulation of cold water (5 °C). Water is dosed by saturation of the gas phase using stainless-steel saturators cooled to 5 °C. The concentration of water vapor in the gas phase at 5 °C and ~1500 mbar pressure is estimated to be ~6000 ppm. For each test 25 mg of the respective photocatalyst were used. Details concerning the photocatalytic cleaning procedure and the actual photocatalytic CO<sub>2</sub> reduction can be found in Ref. [37]. In brief, each catalyst sample was cleaned photocatalytically in an atmosphere containing only gaseous water and helium. This removed hydrocarbon impurities and minimized product formation from carbon sources other than CO<sub>2</sub>.<sup>[36,37]</sup> For testing the activity in photocatalytic CO<sub>2</sub> reduction, each catalyst was brought in contact with a reactant gas mixture of 1.5 % of CO<sub>2</sub> and 0.6 % of H<sub>2</sub>O balanced by He. The addition of H<sub>2</sub>O to the feed gas is enabled by a metal-sealed double saturator which is kept at 5 °C to yield a concentration of about 0.6 % of H<sub>2</sub>O (estimated with the Antoine equation). The reactor was run in the batch mode. The illumination time was 6 h for each experimental run. Initially, the photoreactor was filled with the gas mixture to an overall inside pressure of 1.5 bar. Since the pressure drops by 100 mbar upon each GC sampling, the pressure drops to ~1.1 bar within the course of the measurement.

### Structural Characterization

Diffuse reflectance infrared Fourier transform spectroscopy (DRIFTS) was measured using a Nicolet Protégé 460 spectrometer equipped with praying mantis mirrors and an in situ cell (Harrick HVC-DRP-2). The sample was purged with inert gas throughout the measurement and the temperature was kept at 35 °C. Since TiO<sub>2</sub> is predominantly hydrophilic, inert gas purge is carried out for 1 h before the first spectrum is recorded to remove the majority of physisorbed H<sub>2</sub>O from the catalyst surface.

UV-vis spectroscopy was performed on a Varian Cary 5 G. The Au@TiO<sub>2</sub> materials were suspended in isopropanol prior to measurement. The suspension was loaded into quartz cuvettes and measured in transmission mode.

Transmission electron microscopy (TEM) studies were performed on a Hitachi H-7100 with 100 kV acceleration voltage. Wide angle XRD patterns collected at room temperature were recorded on a Stoe theta/theta diffractometer in Bragg-Brentano geometry (Cu K $\alpha$ <sub>1/2</sub> radiation). The measured patterns were evaluated qualitatively by comparison with entries from the ICDD PDF-2 powder pattern database.

## Acknowledgements

We kindly acknowledge Bernd Spliethoff for the assistance in HR-TEM analysis. This work is partly supported by MAXNET Energy research consortium of the Max Planck Society and the Cluster of Excellence RESOLV (EXC 1069) funded by the Deutsche Forschungsgemeinschaft. Part of this work was funded by the German Ministry of Education and Research (BMBF) within the scope of the funding program "Technologies for Sustainability and Climate Protection – Chemical Processes and Use of CO<sub>2</sub>" (033RC1007A, PhotoKat).

**Keywords:** High-purity photocatalysis • Gold catalysis • Titanium dioxide • Artificial photosynthesis • Core-shell materials

- [1] M. Halmann, *Nature* **1978**, *275*, 115.  
 [2] E. V. Kondratenko, G. Mul, J. Baltrusaitis, G. O. Larrazábal, J. Pérez-Ramírez, *Energy Environ. Sci* **2013**, *6*, 3112.  
 [3] a) M. Haruta, *Catalysis Today* **1997**, *36*, 153–166; b) T. Hayashi, K. Tanaka, M. Haruta, *J. Catal.* **1998**, *178*, 566–575.  
 [4] a) M. C. Holz, K. Kähler, K. Tölle, A. C. van Veen, M. Muhler, *Phys. Status Solidi B* **2013**, *250*, 1094–1106; b) D. Widmann, R. J. Behm, *Acc. Chem. Res* **2014**, *47*, 740–749.  
 [5] a) M. Chen, D. Goodman, *Catalysis Today* **2006**, *111*, 22–33; b) M. Chen, K. Luo, D. Kumar, W. Wallace, C.-W. Yi, K. Gath, D. Goodman, *Surface Science* **2007**, *601*, 632–637.  
 [6] a) M. Comotti, W.-C. Li, B. Spliethoff, F. Schüth, *J. Am. Chem. Soc* **2006**, *128*, 917–924; b) A. S. Wörz, U. Heiz, F. Cinquini, G. Pacchioni, *J. Phys. Chem. B* **2005**, *109*, 18418–18426.  
 [7] a) A. L. Linsebiger, G. Q. Lu, J. T. Yates, *Chem. Rev.* **1995**, *95*, 735–758; b) P. V. Kamat, *J. Phys. Chem. C* **2007**, *111*, 2834–2860; c) A. Kudo, Y. Miseki, *Chem. Soc. Rev.* **2009**, *38*, 253–278; d) F. E. Osterloh, *Chem. Mater.* **2008**, *20*, 35–54; e) X. Li, J. G. Yu, J. X. Low, Y. P. Fang, J. Xiao, X. B. Chen, *J. Mater. Chem. A* **2015**, *3*, 2485–2534; f) J. Yang, D. Wang, H. Han, C. Li, *Acc. Chem. Res.* **2013**, *46*, 1900–1909; g) Y. Ma, X. Wang, Y. Jia, X. Chen, H. Han, C. Li, *Chem. Rev.* **2014**, *114*, 9987–10043  
 [8] A. Lüken, M. Muhler, J. Strunk, *Phys. Chem. Chem. Phys* **2015**, *17*, 10391–10397.  
 [9] B. Mei, C. Wiktor, S. Turner, A. Pougín, G. van Tendeloo, R. A. Fischer, M. Muhler, J. Strunk, *ACS Catal* **2013**, *3*, 3041–3049.  
 [10] G. Dodekatos, H. Tüysüz, *Catal. Sci. Technol.* **2016**, *6*, 7307–7315.  
 [11] S. Schünemann, G. Dodekatos, H. Tüysüz, *Chem. Mater.* **2015**, *27*, 7743–7750.  
 [12] P. Christopher, H. Xin, A. Marimuthu, S. Linic, *Nat Mater* **2012**, *11*, 1044–1050.  
 [13] a) S. Sarina, E. R. Waclawik, H. Y. Zhu, *Green Chem.* **2013**, *15*, 1814–1833; b) G. Dodekatos, S. Schünemann, H. Tüysüz, *Top. Curr. Chem.* **2016**, *371*, 215–252; c) M.A. El-Sayed, *Acc. Chem Res.* **2001**, *34*, 257–264.  
 [14] S. Linic, P. Christopher, D. B. Ingram, *Nat. Mater.* **2011**, *10*, 911–921.  
 [15] K. L. Kelly, E. Coronado, L. L. Zhao, G. C. Schatz, *J. Phys. Chem. B* **2003**, *107*, 668–677.  
 [16] M. Gratzel, *Nature* **2001**, *414*, 338–344.  
 [17] L. Du, A. Furube, K. Yamamoto, K. Hara, R. Katoh, M. Tachiya, *J. Phys. Chem. C* **2009**, *113*, 6454–6462.  
 [18] K. Li, B. S. Peng, T. Y. Peng, *ACS Catal.* **2016**, *6*, 7485–7527.  
 [19] W. Hou, W. H. Hung, P. Pavaskar, A. Goeppert, M. Aykol, S. B. Cronin, *ACS Catal* **2011**, *1*, 929–936.  
 [20] M. Dilla, A. Pougín, J. Strunk, *J. Energy Chem.* **2017**, *26*, 277–283.  
 [21] R. Amrollahi, M. S. Hamdy, G. Mul, *Journal of Catalysis* **2014**, *319*, 194–199.  
 [22] a) E. Ha, L. Y. S. Lee, H. W. Man, S. C. E. Tsang, K. Y. Wong, *ACS Appl. Mater. Interfaces* **2015**, *7*, 9072–9077; b) S. K. Cushing, J. Li, J. Bright, B. T. Yost, P. Zheng, A. D. Bristow, N. Wu, *J. Phys. Chem. C* **2015**, *119*, 16239–16244; c) T. Takata, C. S. Pan, M. Nakabayashi, N. Shibata, K. Domen, *J. Am. Chem. Soc.* **2015**, *137*, 9627–9634; d) B.-H. Wu, W.-T. Liu, T.-Y. Chen, T.-P. Perng, J.-H. Huang, L.-J. Chen, *Nano Energy* **2016**, *27*, 412–419; e) C. H. Li, M. C. Li, S. P. Liu, A. C. Jamison, D. Lee, T. R. Lee, T. C. Lee, *ACS Appl. Mater. Interfaces* **2016**, *8*, 9152–9161; f) Z. W. Seh, S. Liu, M. Low, S.-Y. Zhang, Z. Liu, A. Mlayah, M.-Y. Han, *Adv. Mater.* **2012**, *24*, 2310–2314.  
 [23] a) X. Zhang, Y. Zhu, X. Yang, S. Wang, J. Shen, B. Lin, C. Li, *Nanoscale* **2013**, *5*, 3359–3366; b) S. M. Yoo, S. B. Rawal, J. E. Lee, J. Kim, H.-Y. Ryu, D.-W. Park, W. I. Lee, *Appl. Catal., A* **2015**, *499*, 47–54; c) Y. Q. Sun, Y. G. Sun, T. Zhang, G. Z. Chen, F. S. Zhang, D. L. Liu, W. P. Cai, Y. Li, X. F. Yang, C. C. Li, *Nanoscale* **2016**, *8*, 10774–10782; d) R. Lee, Y. Kumaresan, S. Y.

- Yoon, S. H. Um, I. K. Kwon, G. Y. Jung, *RSC Adv.* **2017**, *7*, 7469-7475; e) Y. Li, J. Zhao, W.-L. You, D. Cheng, W. Ni, *Nanoscale* **2017**, *9*, 3925-3933.
- [24] a) W. G. Tu, Y. Zhou, H. J. Li, P. Li, Z. G. Zou, *Nanoscale* **2015**, *7*, 14232-14236; b) S. Bera, J. E. Lee, S. B. Rawal, W. I. Lee, *Appl. Catal., B* **2016**, *199*, 55-63.
- [25] K. L. Kelly, E. Coronado, L. L. Zhao, G. C. Schatz, *J. Phys. Chem. B* **2003**, *107*, 668-677.
- [26] a) A. Šurca Vuk, R. Ješe, M. Gaberšček, B. Orel, G. Dražič, *Solar Energy Materials and Solar Cells* **2006**, *90*, 452-468; b) J. Soria, J. Sanz, I. Sobrados, J.M. Coronado, A.J. Maira, M.D. Hernández-Alonso, F. Fresno, *J. Phys. Chem. C* **2007**, *111*, 10590-10596; c) S. H. Szczepankiewicz, J. A. Moss, M. R. Hoffmann, *J. Phys. Chem. B* **2002**, *106*, 7654-7658.
- [27] a) J. T. Carneiro, T. J. Savenije, J. A. Moulijn, G. Mul, *J. Phys. Chem. C* **2011**, *115*, 2211-2217; b) P. Du, A. Buenolopez, M. Verbaas, A. Almeida, M. Makkee, J. Moulijn, G. Mul, *Journal of Catalysis* **2008**, *260*, 75-80.
- [28] G. Ramis, G. Busca, V. Lorenzelli, *Materials Chemistry and Physics* **1991**, *29*, 425-435.
- [29] F. Boccuzzi, A. Chiorino, M. Manzoli, *Surface Science* **2000**, *454-456*, 942-946.
- [30] a) L. Mino, A. M. Ferrari, V. Lacivita, G. Spoto, S. Bordiga, A. Zecchina, *J. Phys. Chem. C* **2011**, *115*, 7694-7700; b) C. Deiana, M. Minella, G. Tabacchi, V. Maurino, E. Fois, G. Martra, *Phys. Chem. Chem. Phys.* **2013**, *15*, 307-315; c) H. Noei, L. Jin, H. Qiu, M. Xu, Y. Gao, J. Zhao, M. Kauer, C. Wöll, M. Muhler, Y. Wang, *Phys. Status Solidi B*, **2013**, *250*, 1204-1221; d) W. Grünert, D. Großmann, H. Noei, M.-M. Pohl, I. Sinev, A. De Toni, Y. Wang, M. Muhler, *Angew. Chem. Int. Ed.* **2014**, *53*, 3245-3249.
- [31] M. Dilla, R. Schlögl, J. Strunk, *ChemCatChem* **2017**, *9*, 696-703.
- [32] A. Pugin, A. Lüken, C. Klinkhammer, D. Hiltrop, M. Kauer, K. Tölle, M. Havenith, K. Morgenstern, W. Grünert, M. Muhler, J. Strunk, *Top. Catal.* **2017**, *60*, 1744-1753.
- [33] I. A. Shkrob, T. W. Marin, H. He, P. Zapol, *J. Phys. Chem. C* **2012**, *116*, 9450-9460.
- [34] M. C. Holz, K. Tölle, M. Muhler, *Catal. Sci. Technol.* **2014**, *4*, 3495-3504.
- [35] R. Zanello, S. Giorgio, C. R. Henry, C. Louis, *J. Phys. Chem. B* **2002**, *106*, 7634-7642.
- [36] B. Mei, A. Pugin, J. Strunk, *Journal of Catalysis* **2013**, *306*, 184-189.
- [37] A. Pugin, M. Dilla, J. Strunk, *Phys. Chem. Chem. Phys.* **2016**, *18*, 10809-10817.

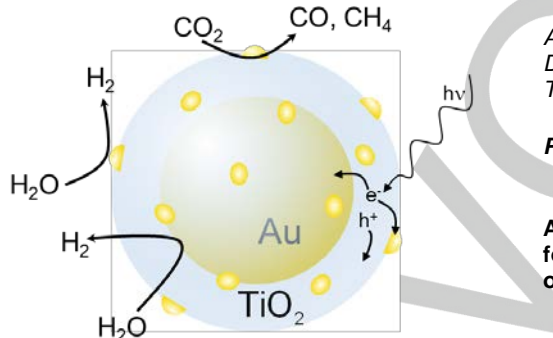
## Entry for the Table of Contents

Layout 1:

## FULL PAPER

**Wrapped up and decorated:**

With Au@TiO<sub>2</sub> core-shell composites featuring additional Au nanoparticles on the outer surface, higher yields of CH<sub>4</sub> and CO can be obtained in photocatalytic CO<sub>2</sub> reduction. Large amounts of H<sub>2</sub> from H<sub>2</sub>O splitting are simultaneously produced. Electronic effects and a catalytic role of gold dominate the performance of the system.



Anna Pougin<sup>[a],†</sup>, Georgios Dodekatos<sup>[b]</sup>, Martin Dilla<sup>[c]</sup>, Harun Tüysüz<sup>[b]</sup>, Jennifer Strunk<sup>[d]</sup>

Page No. – Page No.

**Au@TiO<sub>2</sub> Core-Shell Composites for the Photocatalytic Reduction of CO<sub>2</sub>**